Article

Stabilizing the Central Part of Tropomyosin Increases the Bending Stiffness of the Thin Filament

Salavat R. Nabiev,[1] Denis A. Ovsyannikov,[1] Galina V. Kopylova,[1] Daniil V. Shchepkin,[1] Alexander M. Matyushenko,[2,3] Natalia A. Koubassova,[4] Dmitrii I. Levitsky,[2,5] Andrey K. Tsaturyan,[4] and Sergey Y. Bershitsky[1,*]

[1]Institute of Immunology and Physiology, Russian Academy of Sciences, Yekaterinburg, Russia; [2]A.N. Bach Institute of Biochemistry, Russian Academy of Sciences, Moscow, Russia; [3]Department of Biochemistry, School of Biology, [4]Institute of Mechanics, and [5]A.N. Belozersky Institute of Physico-Chemical Biology, Moscow State University, Moscow, Russia

ABSTRACT A two-beam optical trap was used to measure the bending stiffness of F-actin and reconstructed thin filaments. A dumbbell was formed by a filament segment attached to two beads that were held in the two optical traps. One trap was static and held a bead used as a force transducer, whereas an acoustooptical deflector moved the beam holding the second bead, causing stretch of the dumbbell. The distance between the beads was measured using image analysis of micrographs. An exact solution to the problem of bending of an elastic filament attached to two beads and subjected to a stretch was used for data analysis. Substitution of noncanonical residues in the central part of tropomyosin with canonical ones, G126R and D137L, and especially their combination, caused an increase in the bending stiffness of the thin filaments. The data confirm that the effect of these mutations on the regulation of actin-myosin interactions may be caused by an increase in tropomyosin stiffness.

INTRODUCTION

Contraction of striated muscles is powered by actin-myosin interactions, which are controlled by the regulatory proteins, tropomyosin (Tpm) and troponin (Tn), associated with the actin filaments. Tpm molecules bind each other in a head-to-tail manner (1,2) forming two long helices with a ~36 nm pitch coiling round the actin filament. The Tn complex consisting of three subunits, Tn-C, Tn-I, and Tn-T, binds the Tpm molecules and controls their position on the actin filament: in the absence of Ca^{2+} Tpm sterically blocks the myosin-binding sites on actin, whereas in the presence of Ca^{2+} it releases these sites to enable the binding of myosin heads (1,3).

Although Tpm mainly contains residues characteristic of the canonical heptad repeats, which stabilize the coiled-coil dimer of two α-helices, it has several noncanonical residues that are thought to partially destabilize the dimer. Changes in Tpm properties and the functional role of two noncanonical residues, G126 and D137, located in the central part of the Tpm molecule were recently studied (4–8). Substitution of each of these residues with canonical ones, G126R or D137L, and especially the combination of both these substitutions led to a stabilization of the molecule seen by a suppression of trypsinolysis (4) and an increase in thermal stability as revealed by DSC (5,8). These substitutions also changed the functional properties of the regulated thin filaments containing Tpm mutants: the ATPase rate increased, the Ca^{2+} sensitivity of the actin-myosin interaction also increased, and in a filament-gliding assay the movement of the filaments over a myosin-covered surface was accelerated (4–7). The effects of these substitutions on the mechanical function of the actin-myosin complex in vitro were discussed in terms of a combination of two factors: an increase in the bending stiffness of Tpm and changes in the myosin-Tpm interaction (7,8). However, these hypotheses were not tested directly. It was shown theoretically (9,10) and experimentally (9,11) that the bending stiffness of a Tpm molecule may be an important parameter in the activation of thin filaments, particularly in the propagation of the mechanical wave of activation along the filament.

Here, we use the optical trap technique for measuring the bending stiffness of F-actin and reconstructed regulated thin filaments (consisting of F-actin, Tpm, and Tn complex) to test the effect of the previously mentioned stabilizing mutations in the central part of Tpm. As two continuous Tpm chains reinforce the actin filament, one would expect the total bending stiffness of the reconstructed filament to change in a measurable way upon changes in the Tpm bending stiffness.

Our stiffness analysis is based on the mechanical scheme suggested earlier by Dupuis and colleagues (12). To increase the precision of the measurements we used the exact solution of an elastic mechanical problem instead of the approximate solution used by these authors. We also developed a robust procedure for data analysis.

Submitted April 27, 2015, and accepted for publication June 8, 2015.

*Correspondence: s.bershitsky@iip.uran.ru

Editor: David Warshaw.

0006-3495/15/07/0373/7 $2.00

http://dx.doi.org/10.1016/j.bpj.2015.06.006

MATERIALS AND METHODS

Proteins

All Tpm species used in this work were recombinant proteins that have an Ala-Ser N-terminal extension to imitate naturally occurring N-terminal acetylation of native Tpm (13). Recombinant human Tpm1.1 isoform 1 (α-striated Tpm; according to nomenclature (14)) C190A, D137L/C190A, G126R/C190A, and G126R/D137L/C190A mutants were prepared as described by Matyushenko et al. (7). The C190A mutant was used as a reference that mimics the reduced state of cysteine in the Tmp molecule.

Rabbit skeletal muscle actin was prepared as described (15). F-actin was polymerized by the addition of 2 mM ATP, 4 mM $MgCl_2$, and 100 mM KCl and labeled by rhodamine-phalloidin (Phalloidin-tetramethylrhodamine B, Sigma-Aldrich (St. Louis, MO)). Rabbit skeletal muscle Tn was prepared as described (16).

Optical trap

The dual beam optical trap setup similar to that described by Takagi et al. (17) was built on the base of an inverted fluorescence microscope (AxioObserver, Carl Zeiss Microscopy GmbH (Jena, Germany)) equipped with a high numerical aperture objective (100×, NA 1.25 oil immersed, Carl Zeiss Microscopy GmbH) and a charge-coupled device video camera (CoolSNAPHQ^2, Photometrics, Roper Technologies, Inc. (Sarasota, FL)). A beam of infrared laser (Nd:YLF, 1064 nm wavelength, 5 W; Inversion-Fiber (Novosibirsk, Russia)) was split into two orthogonally polarized beams. The beams focused by the objective produced two independent optical traps in the focal plane inside an experimental flow cell made of a microscope slide and a coverslip. The position of one of the traps, the motor trap, was controlled by an acoustooptical deflector (Neos Technologies, Inc. (Melbourne, FL)). The position of the second, the transducer trap, was fixed. After passing through the flow cell, the beams were collected by a high numerical aperture condenser (NA 1.4, Carl Zeiss Microscopy GmbH) and focused onto two quadrant photodiodes (FD20KP, Russia). The photodiode signals were digitized with a 12-bit ADC (USB3000, R-technology (Moscow, Russia)). The flow cell was mounted on a three-axis piezoplatform (E-761, Physik Instrumente, GmbH (Karlsruhe, Germany) for manipulating its position with 10 nanometer precision in a three-dimensional space.

Experimental protocol and data analysis

Regulated actin filaments were reconstructed from the rhodamine-phalloidin labeled F-actin (0.08 nM), a Tpm mutant (0.1 μM), and Tn (0.1 μM) in the presence of a saturating concentration of Ca^{2+} (~30 μM) or in the absence of Ca^{2+} in the buffer containing: 25 mM KCl, 25 mM imidazole, 4 mM $MgCl_2$, 1 mM EGTA, 20 mM DTT, and oxygen scavenger system (0.5 mg/ml bovine serum albumin, 3.5 mg/ml glucose, 0.02 mg/ml catalase, 0.15 mg/ml glucose oxidase) at pH 7.5. A 6–9-μm-long segment of a reconstructed thin filament was held with its ends between two polystyrene beads (Sigma-Aldrich) of 0.9 μm diameter coated with *N*-ethylmaleimide-treated myosin used as a specific F-actin glue (18) to form a dumbbell. The modification of myosin with *N*-ethylmaleimide and a coating of the polystyrene beads were done according to Veigel et al. (19). The beads of the dumbbell were held by the two laser traps within the flow cell. The dumbbell was stretched by moving the motor bead by a series of 50 nm steps. Signals of the axial displacements of the transducer and motor beads with respect to their traps were recorded for 1 s after each step. The averaged signal of the transducer bead displacement multiplied by the transducer trap stiffness was used as a measure of the average force pulling the dumbbell. The trap stiffness was calculated from the spectrum of the Brownian noise of the transducer bead (20) at the beginning of each stretch cycle when the actin filament in the dumbbell was completely slack.

The distance between the beads was measured from micrographs made with a charge-coupled device camera as shown in Fig. 1. A strip of a micrograph covering both beads was cut along the line connecting the centers of the beads (Fig. 1 *A*). The light intensity of the micrograph was integrated across the strip to obtain the axial intensity profile (Fig. 1 *B*). The positions of the centers of the beads were taken as the coordinates of centers of the intensity peaks of each bead image (Fig. 1 *B*). For this, the center of gravity of the top of the peak above the threshold level (that was set halfway between the peak and its bottom on the intensity profile) was calculated as shown in Fig. 1 *B*. Selection of the strips, integration of the two-dimensional intensity map, and determination of the positions of the peaks from one-dimensional profiles were automated using homemade software. Although the pixel size was 64.4 nm, the accuracy of the peak position determination taking into account the intensity noise in the micrographs (Fig. 1) was significantly less, ~4 nm.

The strain-force diagram was calculated from the measurements of force and the distance between the beads (Fig. 1 *A*). Although 12 steps of 50 nm correspond to a displacement of the motor trap by 12×50 nm $= 0.6$ μm that corresponds to the strain of 600 nm/2/450 nm ≈ 0.667, the observed change $\delta = h/R$ was smaller, only 0.53 because of the existing compliance of the traps and of the filament-to-bead linkages.

The origin of the diagram was rather arbitrary as the initial part of the strain-stress plot is flat and the positions of the beads, which correspond to the position of the slack filament in the initial stages of the stretch, are difficult to determine. We therefore left the origin as a free parameter that should be determined from the experimental data. To estimate the bending stiffness of the thin filament from the strain-force diagram, the diagram was fitted with the theoretical function described below.

At least three different dumbbells were tested with F-actin or with reconstructed regulated thin filaments containing each of the Tpm constructs. Several stretch-release cycles were repeated for each dumbbell. Occasionally the strain-force diagrams contained one, or several steps with an abrupt increase in the bead-to-bead distance accompanied by a relatively small increment in force, or in other cases the strain-force relation remained rather linear and did not show strain saturation even at high forces. We considered such behavior as an indicator of breaking or damaged linkages between a bead and a filament, and these data were omitted from the analysis as the theory used for the data analysis relies on the constancy of the filament length between the points of attachment to the beads. Note that these breaks occurred more often with F-actin than with the regulated thin filaments. The Student's *t*-test and the nonparametric Mann-Whitney

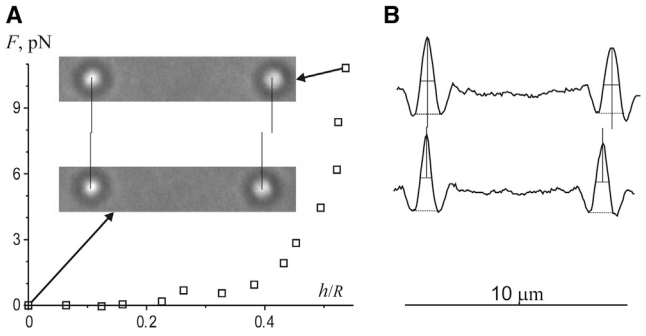

FIGURE 1 Strain-force diagram for a dumbbell containing reconstructed thin filaments containing the C190A Tpm. (*A*) The dependence of the pulling force on the dimensionless strain (*squares*), where h is the change in the half-distance between the beads, and R is the radius of the bead. Inset shows the micrographs of the beads for the first and the last data points before and at the end of the 12-step stretches. The positions of the centers of gravity of the bead images are shown by vertical lines. (*B*) One-dimensional profiles of the light intensity for the bead configurations shown in (*A*). The thresholds for determining the positions of the bead centers and the positions themselves are also indicated by horizontal and vertical lines, respectively.

U-test were used for statistical analysis of the difference in bending stiffness compared to that of the C190A Tpm used as a reference.

Mathematical model

A schematic representation of the configuration of an actin filament bound to one of the beads held by optical trap during stretch of the dumbbell is given in Fig. 2. Without stretch, the filament is straight as its bending moment is zero (*inset* in Fig. 2). Stretch causes filament bending and the simultaneous rotation of the beads so that the tangent points on the beads move closer to each other, the φ angle decreases with the rise of stretching force. The tangent angle θ of the filament decreases progressively and becomes zero on the axis of symmetry between the beads (Fig. 2).

The dependence of the dimensionless force, $\gamma(2FR^2/K)$, where K is the bending stiffness of the filament, on the dimensionless strain, δ, and on another dimensionless parameter that is the ratio of the bead radius to the half-length of the filament segment between the beads, L, $\alpha = R/L$, can be reduced to quadratures (Appendix A). Moreover, calculations show that for $\alpha < 0.25$ the function is practically independent of α, so that it can be expressed by a function $\gamma = f(\delta)$. The function f was calculated numerically and then approximated by a simple formula (Appendix A). Each set of the force-strain data $(\delta_i, \gamma_i), = 1, 2, \ldots, n$ obtained during the stretch cycle of a dumbbell was fitted with this formula using a least squares routine to obtain two fitting parameters, K and δ_0:

$$\delta_i = Kf(\delta_i + \delta_0)/2R^2, \quad (1)$$

where δ_0 is the strain offset due to uncertainty in the origin of the strain-force diagram.

RESULTS

Pooled data are shown in Fig. 3 for several stretch cycles for F-actin and reconstructed thin filaments containing the C190A, G126R/C190A, D137L/C190A, and G126R/D137L/C190A Tpm for at least three different dumbbells for each of the Tpm mutants.

The optimal K values, which provide the least mean square fit (Eq. 1) for individual cycles were averaged to give $3.5 \pm 0.5 \times 10^{-26}$ N·m^2 (here and hereafter mean $\pm$ SE, $n = 11$) for the F-actin, $5.4 \pm 0.6 \times 10^{-26}$ N·m^2 ($n = 7$) for C190A Tpm, and $9.3 \pm 1.0 \times 10^{-26}$ N·m^2 ($n = 6$) for the C190A/G126R/D137L mutants. K values statistics for F-actin and reconstructed thin filaments with Tpm mutants in the absence and presence of a saturating concentration of Ca^{2+} is summarized in Table 1.

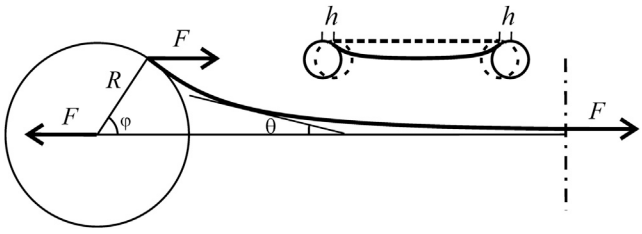

FIGURE 2 Two beads of radii R held by optical traps are connected by an actin filament (*bold line*) to form a dumbbell as shown in the inset; the solid lines show the bead positions and the configuration of the filament under stretch of the dumbbell by a tensile force F. The unstrained positions of the beads and configuration of the filament are shown by the dashed lines. The middle of the filament is shown in the stretched and nonstretched dumbbell positions to symmetrize the picture. The left bead and a half of the filament are shown on an expanded scale; the symmetry plane is shown as a dot-dash vertical line on the right. The, stretching force, F, and the angle to the point of filament attachment on the bead, φ, are also shown.

The addition of C190A Tpm and Tn to F-actin induced a statistically significant 54% increase in the bending filament stiffness (Table 1).

The presence of the D137L/C190A Tpm and especially G126R/D137L/C190A Tpm lead to a further increase in the bending stiffness of the reconstructed thin filaments compared to that with the C190A Tpm mutant. The G126R/C190A mutations in Tpm also induced an increase in the bending stiffness, although it was not statistically significant. The data show that stabilizing mutations in the central part of Tpm induce measurable increases in the stiffness of reconstructed thin filament. Surprisingly, the filament stiffness did not increase in the absence of Ca^{2+}. Under these conditions, Tn binds to the actin filament, shifting the position of the Tpm strand on the thin filament, thereby switching the activated regulated filament to the blocked state. We found that in the absence of Ca^{2+} there was a tendency (though statistically insignificant) for a decrease in stiffness with both C190A and G126R/D137L/C190A Tpm mutants (Table 1).

DISCUSSION

Comparison with previous studies

For the first time, changes in the flexural rigidity of thin filaments induced by the presence of Tpm have been assessed by the spectroscopy of elastic light scattering (21,22). Currently, there are two approaches to measure the flexing rigidity of actin filaments. The first is based on the analysis of the Brownian bending motion of the filaments, using the wormlike chain (WLC) theory (e.g., 23–26). The other is the direct measurements of the strain-force relation of a segment of a filament with a two-beam optical trap developed by Dupuis et al. (12). The theory used for quantitative analysis of these data considers actin filament as an elastic bar with a uniform bending stiffness. Dupuis et al. (12) showed that filament stretch is accompanied by a rotation of the beads similar to that illustrated in Fig. 1. The approximate theory they used was based on an assumption that the shape of the bent segment of an actin filament can be approximated with an arc of a circle. The theory was applied to the data presented as the dumbbell compliance plotted against stretch force. The best fit corresponded to the K value $1.53 \pm 0.37 \times 10^{-26}$ N·m^2 for rhodamine-phalloidin F-actin.

We used the same approach for studying the bending stiffness of actin filament reinforced by Tpm. Several improvements were introduced. An exact solution of the elastic problem was obtained instead of the approximate one

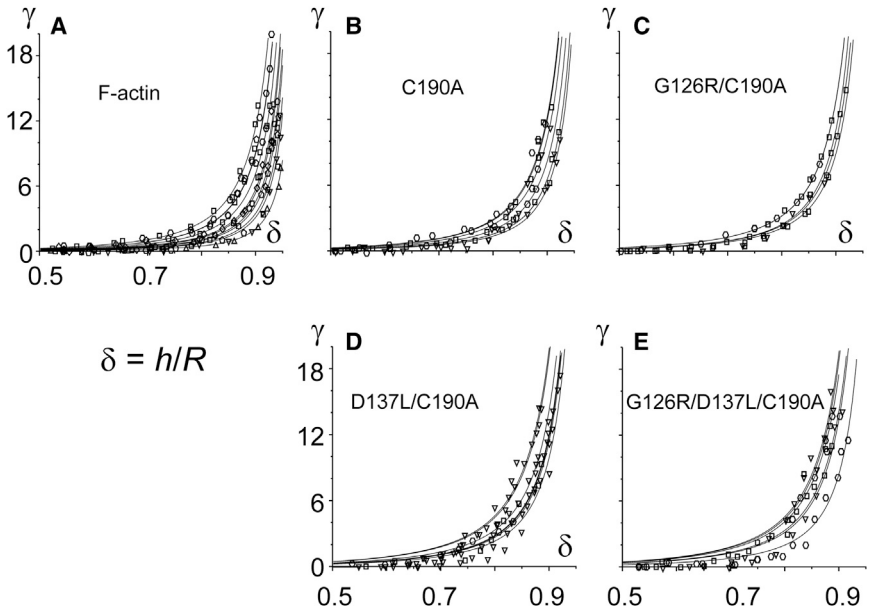

FIGURE 3 Pooled data for the fitted strain-force diagrams obtained from several stretch cycles for at least three dumbbells (shown by *different symbols*) for F-actin (*A*) and reconstructed thin filaments containing either Tpm C190A (*B*) or Tpms G126R/C190A (*C*), D137L/C190A (*D*), and G126R/D137L/C190A (*E*). Continuous lines are the theoretical fitting curves calculated with Eq. 1 using optimized parameters K and δ_0, which provide the least mean-square deviation from the data points. Averaged traces for all panels (*A–E*) are presented in Fig. S1.

employed by Dupuis et al. (12). The bead displacement was measured directly from the micrographs instead of its estimation from the signal of the bead held by the movable trap. This estimation is based on the assumption that the trap stiffness is constant. However, the stiffness of the movable trap changes with its position. For this reason direct measurement of the distance between the beads is more reliable. The displacement of the bead in the fixed beam with constant stiffness corresponded to the force signal. In addition, the bending stiffness was estimated here from the raw strain-force relation, not from the tension-compliance relation used by Dupuis with colleagues (12) as the calculation of the dumbbell compliance (i.e., the derivative of the noisy force and displacement data) increases noise. These improvements notably increase the precision of the method (Fig. S1 in the Supporting Material).

The rigidity of the rhodamine-phalloidin-labeled F-actin estimated by Dupuis et al. (12) is ~43% of that found here. This difference can be explained by the differences in the theories used for data interpretation (Fig. S1) and data analysis procedures.

Another approach for measuring the bending stiffness of actin filaments is based on the visualization of the filaments subjected to the Brownian bending and data analysis with the WLC theory (9,11,23–27). The major parameter in the WLC theory is the persistence length, L_p, which is determined by the bending stiffness K and absolute temperature T: $L_p = K/k_BT$, where k_B is the Boltzmann constant. Several groups measured L_p (and therefore K) using approaches developed by Gittes et al. (24) and Ott et al. (25) by measuring the parameters of Brownian fluctuations from the shape changes of fluorescently labeled actin filaments. For rhodamine-phalloidin actin filaments, the estimations for K were 7.3×10^{-26} N·m^2 (24) and 7.0×10^{-26} N·m^2 (25). Isambert et al. (26) also estimated K to be between 6.5×10^{-26} N·m^2 and 8×10^{-26} N·m^2 depending on polymerization conditions. These figures are about twice that found here for the same preparation of F-actin.

Binding of Tpm (with or without Tn) induced an increase in the flexural rigidity of F-actin by a factor of 1.5–2, if F-actin did not contain phalloidin (21,26–28). The K values varied from 3.7×10^{-26} N·m^2 for F-actin without Tpm to $7.4–8.8 \times 10^{-26}$ N·m^2 for F-actin Tpm complex (26,27). If Tn was added, K increased from 5.1 in the presence of Ca^{2+} to 8.5 without it (26). A stiffening of the reconstructed thin filaments upon Ca^{2+} removal has also been found using the light scattering spectroscopy (22).

When F-actin was reinforced by phalloidin, addition of Tpm had little if any effect on its bending stiffness (26). In our experiments K of rhodamine-phalloidin F-actin increased by 40% without Ca^{2+} and by 54% with Ca^{2+} upon addition of Tpm and Tn (Table 1).

We can therefore conclude that our estimates of K are lower than those obtained by applying the WLC theory to

TABLE 1 Bending stiffness of F-actin and reconstructed thin filaments with Tpm mutants

Filaments	Bending Stiffness, $K \times 10^{26}$ N·m^2, Mean ± SE (Full Range, *n*)	
F-actin	3.5 ± 0.5 (1.3–5.6, *11*)[a,b]	
with Tpm and Tn	$+Ca^{2+}$	$-Ca^{2+}$
C190A	5.4 ± 0.6 (3.5–7.5, *7*)	4.9 ± 0.8 (3.7–7.4, *7*)
G126R/C190A	6.9 ± 0.6 (5.6–8.4, *5*)	
D137L/C190A	8.0 ± 0.8 (6.0–12.1, *7*)[a,b]	
G126R/D137L/C190A	9.3 ± 1.0 (5.2–11.9, *6*)[a,b]	8.3 ± 1.3 (6.3–14.9, *6*)[b]

The significance of the difference from the C190A Tpm mutant in the presence of Ca^{2+} at $p < 0.05$ for the Student's *t*-test ([a]) and the Mann-Whitney U-test ([b]) are shown.

the Brownian bending of actin filaments, although our estimates are significantly higher than those reported earlier (12) with the use of optical trap.

Merits and limitations of the optical trap method for measuring bending stiffness

We believe that the difference between the K values estimated here and those obtained from the WLC theory is caused by a limitation in the accuracy of the quantitative description of the shape of a bent filament. The apparent width of the fluorescent filament images is several hundred nanometers due to the diffraction limit. Thus, high-frequency small-amplitude fluctuations in the shape are unavoidably smoothed. For this reason the estimation of L_p based on measurement of the tangent angles along the filament (25) leads to an underestimation of the angle between the tangents at different filament points and therefore to an overestimation of K. In addition, even in a narrow flow cell, 1.5–3 mm deep, Brownian bending of a filament is three-dimensional: data analysis assuming that a filament is confined to two-dimensional (26) may cause additional errors.

The method exploited here requires a rather sophisticated setup. However, with it, the force and bead displacement measurements are straightforward, data analysis is automated, and sample-to-sample statistics can be collected. Although the data quality critically depends on the robustness of the bead-to-filament links and data selection is needed to obtain reliable and reproducible results, the sensitivity of the method allowed us to determine changes in the filament stiffness caused by the substitution of one or two residues.

Our model assumes that Brownian bending motion has a negligible effect on the distance between the ends of an actin filament in the dumbbell, and the problem can be formulated in terms of a classical theory of elasticity (Appendix A). To validate this assumption we estimated the shortening of the unstretched filament caused by Brownian bending, and the apparent stiffness associated with the filament straightening upon stretch as follows. The root mean-square distance between the points of filament attachment to the beads, L_{RMS}, is given by the formula (29):

$$L_{RMS} = \frac{L}{\varepsilon}\sqrt{2(\varepsilon - 1 + \exp(-\varepsilon))},$$

where $\varepsilon = L/L_p$, L is a half-length of the filament segment between the beads. In our experiments L was in the range of 3–4.5 μm and L_p was between 10 and 20 μm, so that ε ranged from 0.15 to 0.45. Therefore, the difference between L and L_{RMS} can be calculated using Taylor series expansion:

$$L - L_{RMS} = L - L\sqrt{1 - \frac{\varepsilon}{3}} = \frac{L\varepsilon}{6},$$

or 0.075 to 0.34 μm. The corresponding δ value was therefore in the range of 0.17–0.75. The apparent tensile stiffness, S_a, associated with straightening of the thermally shortened filament in the stiff approximation ($\varepsilon < 1$) can be described as (30): $S_a = K^2/(k_B T L^4)$. Using the range of L and K values in our experiments, S_a is calculated to be between 1 and 26 fN/μm. As this value is negligibly small compared to the apparent dumbbell stiffness found in our experiments (Fig. 1), one can neglect this effect and use only the elasticity theory, and ignore Brownian filament bending.

As the force level needed to straighten the filament was far below the resolution limit of our experiments, the offset of the strain-force curve of the straightened filament, δ_0, should be left as a free parameter. We therefore started a stretch cycle at a bead-to-bead distance where no measurable force or significant correlation between the Brownian motion of two beads was detected. We then performed step stretches of the dumbbell until obvious signs of breakage in the bonds between the filament and a bead were observed. A breaking event was detected by a large increase in the distance between the beads without a significant increase in force. To avoid more subtle effects of bond breakage on the results of our analysis we selected only those stretch cycles where the dumbbell length saturated, despite further increases in force, and also ignored stretch cycles where the strain-force diagram remained linear, even at high force.

Implications of the results

Our data confirm that the substitutions of the Tpm residues G126 and D137 with the canonical ones, Arg and Leu, respectively, increase the stiffness of the Tpm coiled-coil. The stiffening of the reconstructed actin filaments in the presence of these mutants reported can be attributed to an increase in the bending stiffness of Tpm as the other parameters such as the actin filaments and the experimental conditions remained unchanged for all Tpm constructs. The more pronounced effect of the D137L mutation compared to the G126R Tpm mutant may be caused by the different positions of these two residues in the heptad repeat within the coiled-coil Tpm structure. Although the noncanonical residue D137 is localized at the position d of the coiled-coil where a hydrophobic residue is normally present, the G126 residue is at the g position that normally is occupied by a charged residue that participates in a weaker electrostatic interaction with an oppositely charged residue of the paired Tpm chain. A similar interpretation explains the increase in thermal stability of the G126R and D137L Tpm mutants compared to the wild-type protein (8). As one would expect, the substitution of both D137 and G126 residues with canonical ones induced an enhanced increase in the bending stiffness of the reconstructed regulated actin filaments. Our findings are in accordance with the observed increase in thermal stability (5,8) and decrease in trypsin cleavage (4) of these mutants. Filament stiffening correlates well with the increased Ca-sensitivity of the sliding velocity

of the regulated thin filament containing these mutants in the actin-myosin in vitro motility assay (6,7).

CONCLUSIONS

We demonstrate a method for determining the bending stiffness of actin filaments using a two-beam optical trap. The method relies on the direct measurement of changes in the bead-to-bead distance caused by applied forces, and subsequent fit of the data to an exact solution of an elastic problem. The resolution of the method is sufficient to distinguish the effect of one or two point mutations in the Tpm molecules on the stiffness of reconstructed thin filaments. The results confirm our assumption that changes in the actin-myosin interaction and its regulation by Ca^{2+} ions caused by the stabilizing mutations in the central part of the Tpm molecule (6,7) may result from an increase in Tpm bending stiffness possibly by an increase in the effective length of the regulatory unit (4,10).

APPENDIX A: MATHEMATICAL MODEL

We denote θ the angle between the tangent line of the actin filament and the line connecting the centers of the two beads of the dumbbell (Fig. 2). The equilibrium equation of the actin filament that is considered as an inextensible elastic bar can be written as (31).

$$K\frac{d^2\theta(s)}{ds^2} - F\sin\theta(s) = 0, \tag{A1}$$

where K is the bending stiffness and s is the natural parameter or the distance along the actin filament measured from the point of its attachment to the left bead (Fig. 2). The boundary conditions for Eq. A1 are as follows (see also Fig. 2):

$$\theta(0) = \frac{\pi}{2} - \varphi,\ \theta(L) = 0, \tag{A2}$$

where L is the half-length of the segment of the actin filament between the points of its attachment to the beads and φ is the angle between the directions toward the second bead and toward the point of the filament attachment (Fig. 2).

Multiplying Eq. A1 by $d\theta(s)/ds$, integrating it over s and using the boundary condition Eq. A2 one obtains

$$\frac{K}{2F}\left(\frac{d\theta(s)}{ds}\right)^2 + \cos\theta(s) = \text{const} = \frac{K}{2F}\left(\frac{d\theta(s)}{ds}\right)^2 + \sin\varphi. \tag{A3}$$

As the total torque applied to the bead should be zero, we additionally have

$$\frac{K}{R}\frac{d\theta(s)}{ds} + RF\sin\varphi = 0.$$

We then introduce dimensionless parameters: the natural parameter x along the filament, $x = s/R$ and the normalized stretching force, $\gamma = 2FR^2/K$, to give the solution of Eq. A3 in the form

$$x = 2\int_{\theta}^{\frac{\pi}{2}-\varphi} \frac{d\theta}{\sqrt{\gamma^2\sin^2\varphi + 4\gamma(\sin\varphi - \cos\theta)}}, \tag{A4}$$

which represents an elliptical integral. Substituting Eq. A4 into Eq. A2 gives the identity:

$$\frac{1}{\alpha} = 2\int_{0}^{\frac{\pi}{2}-\varphi} \frac{d\theta}{\sqrt{\gamma^2\sin^2\varphi + 4\gamma(\sin\varphi - \cos\theta)}}, \tag{A5}$$

where $\alpha = R/L$ is a constant. For the given values of α and γ, Eq. A5 determines φ as a function of the stretching force F. The dimensionless displacement $\delta = h/R$ (where h is the displacement of each bead with respect to the center of the dumbbell caused by the stretch as shown in the *inset* in Fig. 2) can then be calculated as follows:

$$\delta = \cos\varphi - \frac{1}{\alpha} + 2\int_{0}^{\frac{\pi}{2}-\varphi} \frac{d\theta}{\sqrt{\gamma^2\sin^2\varphi + 4\gamma(\sin\varphi - \cos\theta)}}. \tag{A6}$$

Computer calculations show that for $\alpha < 0.25$ (i.e., for beads of 0.9 μm diameter a filament length should be longer than 3.6 μm) the relationship between γ and δ is practically independent of α. The dependence of the dimensionless force, γ, on the dimensionless bead displacement, δ, for small α calculated numerically from Eq. A6 with the additional condition Eq. A5 is shown in Fig. 4 together with its simple approximation:

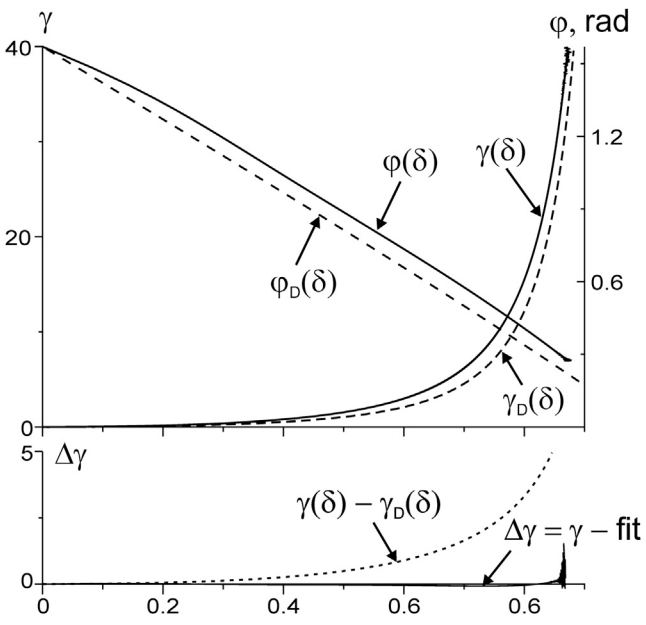

FIGURE 4 The theoretical dependence of the dimensionless force, γ, and angle, φ, on the dimensionless bead displacement, δ, obtained by computer calculations using the theory developed here are shown by continuous lines. The same dependencies calculated with the theory of Dupuis et al. (12) are denoted with subscript index D and shown by dashed lines. The difference, $\Delta\gamma$, between the computer calculated γ value and its approximation is shown in the bottom plot by a continuous line. It is <0.12, i.e., lies within the precision of our experiments. Dotted line shows the difference between the two theories.

$$\gamma(\delta) = a_1\left(a_2\delta^2 - \delta + a_3\left(1 - \frac{1}{(1-\delta)^2}\right)\right),$$

where $a_1 = 1.2139$, $a_2 = 0.385$, $a_5 = 0.555$, which provides quite a good fit (Fig. 4).

For practical convenience we used the approximate theoretical function γ for data fitting instead of the more precise one obtained from the numerical solution.

SUPPORTING MATERIAL

One figure is available at http://www.biophysj.org/biophysj/supplemental/S0006-3495(15)00588-3.

AUTHOR CONTRIBUTIONS

S.N. built the setup, performed research, and analyzed data; D.O. contributed setup control software; G.K. and D.S. prepared actin and troponin; A.M. prepared tropomyosin mutants; N.K. contributed analytic tools and analyzed data; D.L. prepared tropomyosin mutants; A.T. designed research, analyzed data, and wrote the article; S.B. built the setup, designed research, and wrote the article.

ACKNOWLEDGMENTS

The authors thank Mr. Feodor Syomin for help in software development and Prof. M.A. Ferenczi for critical reading of the manuscript and useful discussion.

This work was supported by the Russian Foundation for Basic Research (RFBR) grants 13-04-40101-N (to S.B.), 13-04-40099-N (to D.L.), 13-04-40100-N (to A.T.), 15-04-02174 (to N.K.), and the Program "Molecular and Cell Biology" of the Russian Academy of Sciences (to D.L.).

REFERENCES

1. Nevzorov, I. A., and D. I. Levitsky. 2011. Tropomyosin: double helix from the protein world. *Biochemistry (Mosc).* 76:1507–1527.
2. Orzechowski, M., X. E. Li, …, W. Lehman. 2014. An atomic model of the tropomyosin cable on F-actin. *Biophys. J.* 107:694–699.
3. McKillop, D. F. A., and M. A. Geeves. 1993. Regulation of the interaction between actin and myosin subfragment 1: evidence for three states of the thin filament. *Biophys. J.* 65:693–701.
4. Sumida, J. P., E. Wu, and S. S. Lehrer. 2008. Conserved Asp-137 imparts flexibility to tropomyosin and affects function. *J. Biol. Chem.* 283:6728–6734.
5. Nevzorov, I. A., O. P. Nikolaeva, …, D. I. Levitsky. 2011. Conserved noncanonical residue Gly-126 confers instability to the middle part of the tropomyosin molecule. *J. Biol. Chem.* 286:15766–15772.
6. Shchepkin, D. V., A. M. Matyushenko, …, D. I. Levitsky. 2013. Stabilization of the central part of tropomyosin molecule alters the Ca^{2+}-sensitivity of actin-myosin interaction. *Acta Naturae.* 5:126–129.
7. Matyushenko, A. M., N. V. Artemova, …, D. I. Levitsky. 2014. Structural and functional effects of two stabilizing substitutions, D137L and G126R, in the middle part of α-tropomyosin molecule. *FEBS J.* 281:2004–2016.
8. Matyushenko, A. M., N. V. Artemova, …, D. I. Levitsky. 2015. Effects of two stabilizing substitutions, D137L and G126R, in the middle part of α-tropomyosin on the domain structure of its molecule. *Biophys. Chem.* 196:77–85.
9. Li, X. E., W. Suphamungmee, …, W. Lehman. 2012. The flexibility of two tropomyosin mutants, D175N and E180G, that cause hypertrophic cardiomyopathy. *Biochem. Biophys. Res. Commun.* 424:493–496.
10. Metalnikova, N. A., and A. K. Tsaturyan. 2013. A mechanistic model of Ca regulation of thin filaments in cardiac muscle. *Biophys. J.* 105:941–950.
11. Loong, C. K., M. A. Badr, and P. B. Chase. 2012. Tropomyosin flexural rigidity and single Ca2+ regulatory unit dynamics: implications for cooperative regulation of cardiac muscle contraction and cardiomyocyte hypertrophy. *Front. Physiol.* 3:80.
12. Dupuis, D. E., W. H. Guilford, …, D. M. Warshaw. 1997. Actin filament mechanics in the laser trap. *J. Muscle Res. Cell Motil.* 18:17–30.
13. Monteiro, P. B., R. C. Lataro, …, Fde. C. Reinach. 1994. Functional alpha-tropomyosin produced in *Escherichia coli*. A dipeptide extension can substitute the amino-terminal acetyl group. *J. Biol. Chem.* 269:10461–10466.
14. Geeves, M. A., S. E. Hitchcock-DeGregori, and P. W. Gunning. 2014. A systematic nomenclature for mammalian tropomyosin isoforms. *J. Muscle Res. Cell Motil.* 36:147–153.
15. Pardee, J. D., and J. A. Spudich. 1982. Purification of muscle actin. *Methods Cell Biol.* 24:271–289.
16. Potter, J. D. 1982. Preparation of troponin and its subunits. *Methods Enzymol.* 85:241–263.
17. Takagi, Y., E. E. Homsher, …, H. Shuman. 2006. Force generation in single conventional actomyosin complexes under high dynamic load. *Biophys. J.* 90:1295–1307.
18. Meeusen, R. L., and W. Z. Cande. 1979. *N*-ethylmaleimide-modified heavy meromyosin. A probe for actomyosin interactions. *J. Cell Biol.* 82:57–65.
19. Veigel, C., M. L. Bartoo, …, J. E. Molloy. 1998. The stiffness of rabbit skeletal actomyosin cross-bridges determined with an optical tweezers transducer. *Biophys. J.* 75:1424–1438.
20. Neuman, K. C., and S. M. Block. 2004. Optical trapping. *Rev. Sci. Instrum.* 75:2787–2809.
21. Fujime, S., and S. Ishiwata. 1971. Dynamic study of F-actin by quasielastic scattering of laser light. *J. Mol. Biol.* 62:251–265.
22. Ishiwata, S., and S. Fujime. 1972. Effect of calcium ions on the flexibility of reconstituted thin filaments of muscle studied by quasielastic scattering of laser light. *J. Mol. Biol.* 68:511–522.
23. Yanagida, T., M. Nakase, …, F. Oosawa. 1984. Direct observation of motion of single F-actin filaments in the presence of myosin. *Nature.* 307:58–60.
24. Gittes, F., B. Mickey, …, J. Howard. 1993. Flexural rigidity of microtubules and actin filaments measured from thermal fluctuations in shape. *J. Cell Biol.* 120:923–934.
25. Ott, A., M. Magnasco, …, A. Libchaber. 1993. Measurement of the persistence length of polymerized actin using fluorescence microscopy. *Phys. Rev. E Stat. Phys. Plasmas Fluids Relat. Interdiscip. Topics.* 48:R1642–R1645.
26. Isambert, H., P. Venier, …, M. F. Carlier. 1995. Flexibility of actin filaments derived from thermal fluctuations. Effect of bound nucleotide, phalloidin, and muscle regulatory proteins. *J. Biol. Chem.* 270:11437–11444.
27. Greenberg, M. J., C. L. Wang, …, J. R. Moore. 2008. Modulation of actin mechanics by caldesmon and tropomyosin. *Cell Motil. Cytoskeleton.* 65:156–164.
28. Goldmann, W. H. 2000. Binding of tropomyosin-troponin to actin increases filament bending stiffness. *Biochem. Biophys. Res. Commun.* 276:1225–1228.
29. Kroy, K., and E. Frey. 1996. Force-extension relation and plateau modulus for wormlike chains. *Phys. Rev. Lett.* 77:306–309.
30. MacKintosh, F. C., J. Käs, and P. A. Janmey. 1995. Elasticity of semiflexible biopolymer networks. *Phys. Rev. Lett.* 75:4425–4428.
31. Landau, L. D., and E. M. Lifshitz. 1975. Theory of Elasticity, 2nd English ed. Pergamon Press, Oxford, UK.